Bioprinting 17 (2020) e00066

Contents lists available at ScienceDirect

Bioprinting

journal homepage: www.elsevier.com/locate/bprint

Research paper

3D printing multiphasic osteochondral tissue constructs with nano to micro features via PCL based bioink

Margaret Nowicki [a,*], Wei Zhu [b], Kausik Sarkar [b], Raj Rao [c], Lijie Grace Zhang [b,d,e,f]

[a] Department of Civil and Mechanical Engineering, The United States Military Academy, West Point, NY, 10996, USA
[b] Department of Aerospace and Mechanical Engineering, The George Washington University, Washington, DC, 20052, USA
[c] Department of Orthopedic Surgery, The George Washington University, Washington, DC, 20052, USA
[d] Department of Biomedical Engineering, The George Washington University, Washington, DC, 20052, USA
[e] Department of Electrical and Computer Engineering, The George Washington University, Washington, DC, 20052, USA
[f] Department of Medicine, The George Washington University, Washington, DC, 20052, USA

ARTICLE INFO

Keywords:
3D printing
Bioink
Osteochondral
Stem cells

ABSTRACT

Osteochondral tissue has a complex graded structure where biological, physiological, and mechanical properties vary significantly over the full thickness spanning the subchondral bone region beneath the joint surface to the hyaline cartilage region at the joint surface. This presents a significant challenge for tissue-engineered structures addressing osteochondral defects. Advanced bioinks, together with 3D bioprinters, may present a unique solution to this problem. The objective of this research is to apply innovative bioinks, and integrate fused deposition modeling (FDM) 3D printing with a casting technique to fabricate novel osteochondral tissue constructs for improved bone marrow human mesenchymal stem cell (hMSC) functions. Specifically, a multiphasic construct with different layer geometries was designed. A polycaprolactone (PCL) based shape memory material which is comprised of polycaprolactone-triol, castor oil, and poly(hexamethylene diisocyanate) was used as the osteochondral matrix material for the first time. Nanocrystalline hydroxyapatite (nHA) was synthesized and printed into the subchondral bone layers and chondrogenic growth factors were fabricated into the cartilage layer. The results show that the 3D printed constructs with nHA and bioactive cues have improved mechanical properties and enhanced hMSC adhesion, growth, and differentiation. This study indicates that both mechanical properties and cell performance can be easily manipulated through the bioink and the investment casting process to achieve a spatially appropriate osteogenic and chondrogenic response in engineered osteochondral constructs.

1. Introduction

Osteochondral repair is a blend of both cartilage and bone tissue engineering. Careful consideration of the needs of both regions is essential in fabricating successful osteochondral tissue constructs. Osteochondral design is often closely linked with, or driven by, cartilage repair because of the challenges inherent with cartilage regeneration; some research also suggests that cartilage and subchondral bone should be considered interdependent when addressing osteochondral defects and repair [1,2]. Native osteochondral tissue, along with cartilaginous tissue, lacks significant vascularity [3]. The lack of vascular networks hinders effective nutrient transport. This, along with the inherent compositional complexity of the tissue are the primary underlying reasons it is so difficult to effectively repair this region.

Hyaline cartilage is a smooth connective tissue covering the articular surface of joints to minimize friction. It is mainly composed of type II collagen, is void of nerves and blood cells, and has a limited capacity to regenerate and self-repair. Damaged hyaline cartilage is often replaced with fibrocartilage, which possesses completely different physical and mechanical properties [4]. To successfully design and construct a biomimetic osteochondral interface it is necessary to evaluate both the chondrogenic and osteogenic performance of the scaffold, with chondrogenic being more challenging. As such, this work focuses on integrating an innovative bioink by first concentrating on chondrogenic performance, then transitioning to biphasic osteochondral performance.

Rapid prototyping technologies via additive manufacturing, and specifically 3D bioprinting, can readily enable physicians to efficiently engineer personalized constructs for patient-specific treatment [5–7]. Ultimately, patients will not have to wait for a viable donor or surrender

* Corresponding author.
E-mail address: margaret.nowicki@westpoint.edu (M. Nowicki).

https://doi.org/10.1016/j.bprint.2019.e00066
Received 18 May 2019; Received in revised form 7 September 2019; Accepted 25 September 2019
2405-8866/Published by Elsevier B.V.

to total joint replacement at an early age due to disease progression but will instead be treated with cell-laden or bioactive 3D constructs. Advances in biomaterials research is critical to the realization of functional and efficient scaffolding where processability and biocompatibility must be taken into consideration. One of the fastest and least expensive methods of 3D construct fabrication is fused deposition modeling (FDM). It is the bottom-up, layer-by-layer extrusion of a thermoplastic polymer filament yielding rigid structures [8]. The printer nozzle moves along the x- and y-axis while the printing platform lowers in the z-axis. While this technology is rapid, it has limitations. Most notably, structural stability challenges in designs with horizontal channels (x- and y-axis) or overhangs exist due to the bottom up approach and viscosity of the extruded filament. Soluble support material can be used for designs where overhangs require external support until the extruded filament cools to a temperature where it is capable of self-support.

The commercial availability of printable filaments is fairly broad, but availability of biomaterial filaments is still limited. Additionally, less robust polymers often require a difficult to achieve balance between temperature and extrusion speed to give an optimal result. The limiting force when utilizing FDM is often the ramming force, i.e. a force generated by the drive wheel as the filament is fed into the heated nozzle [9]. Temperature controls the viscosity and flow rate of the extruding filament and must be carefully balanced with ramming force to prevent filament kinking on the forcing end or rapid flow-rate at the nozzle tip. More research is needed to tune FDM-based printers to extend their capabilities to process more biocompatible materials like polycaprolactone (PCL), especially given the proven positive *in vivo* response of this material.

Even though material limitations persist for FDM-based printers, it still remains one of the more reliable fabrication methods for creating various robust tissue engineering constructs. Compared to other printing methods, it produces constructs with favorable mechanical strength that are customizable, reproducible, and support cell growth. Additionally, the customizable nature of FDM constructs supports their applications as a mold for an investment casting technique. This process integrates FDM printed molds with crosslinkable polymer bioinks to create favorable constructs for various tissue engineering applications. Investment casting facilitates easy integration of bioactive factors, such as nano hydroxyapatites (nHA, bone minerals) and transforming growth factors, to affectively direct cellular differentiation. It also opens the door for numerous cross-linkable bioink resins such as the PCL-triol material investigated herein. In this study, a multiphasic 3D mold was designed and generated by an FDM printer. The casting technique was then adopted to obtain the ultimate osteochondral constructs with tunable mechanical properties and bioactive cues. The osteogenic and chondrogenic responses of hMSCs grown in the constructs were examined.

2. Materials and methods

2.1. Nano hydroxyapatite synthesis

nHA was synthesized using a wet chemical precipitation method, followed by a hydrothermal treatment [10,11]. First, 75 mL of ammonium phosphate (0.6 M) (Sigma Aldrich, St. Louis, MO) was added to 750 mL of water. Ammonium hydroxide (Fisher Scientific, Pittsburg, PA) was then added to adjust the pH to 10. Next, 1 M calcium nitrate (Sigma Aldrich, St. Louis, MO) was added while stirring at a rate of 5 mL/min, then the solution sat for 10 min at room temperature to allow precipitation to occur. The HA mixture was treated at 200 °C for 20 h in a Teflon liner within an acid digestion chamber (Parr Instrument Company, Moline, IL). After the hydrothermal treatment, the resultant nHA solution was centrifuged and washed 3 times. Lastly the nHA particles were dried in an 80 °C oven for 12 h and then ground into a fine powder.

2.2. Osteochondral scaffold design and fabrication

Fig. 1 illustrates the architecture of human osteochondral tissue found at the surface of articulating joints and our computer aided design (CAD) images used to create the multiphasic mold for this region. The dimensions of each layer were designed using guidance from various sources outlining thickness of articular cartilage as well as the percent thickness of each sub layer. The designed thickness for the layer on the cartilage side was 3 mm and for the bone side was 1.8 mm, 0.3 mm per layer, for a scaffold thickness of 4.8 mm. The 0.6 mm difference between actual scaffold and mold is accounted for with the two layers of solid sacrificial mold required to prevent the resin from leaking out of the bottom during the investment casting process.

Specifically, square molds measuring 35 mm × 35 mm × 5.4 mm (length × width × height) for investment casting were drawn using CAD software and prepared for 3D printing by computer numerical control (CNC) software. Overall mold thickness and geometry of each sample remained constant for all sample groups. Modification of the CNC file to vary infill density allows precise control of pore distribution, alignment, and density. The pore distribution was designed and fabricated to transition over the entirety of the scaffold thickness, replicating pore distributions and alignments similar to native articular cartilage [3]. Moving vertically, the pore and channel geometries transitioned to allow a biomimetic vertical alignment of cells in the lower third, a randomized distribution of cells in the middle, and a horizontal distribution of cells on the surface of the scaffold.

Fig. 2 illustrates the scaffold fabrication process. Firstly, water soluble polyvinyl alcohol (PVA) was FDM printed into leachable molds. After printing, a thermally sensitive smart shape memory resin that is comprised of PCL-triol and castor oil with a 40:60 molecular weight ratio, and a poly (hexamethylene diisocyanate) crosslinking agent, was cast

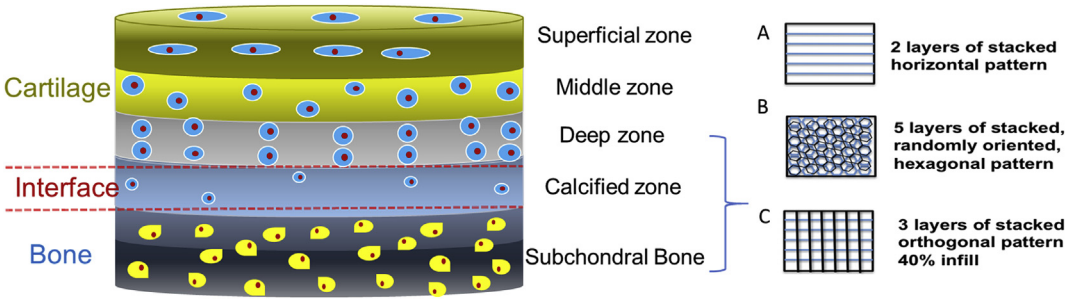

Fig. 1. Schematic representation of an osteochondral region with our scaffold mold designs representing each layer (not drawn in scale). (A) The superficial region contains horizontally aligned cells and fibers and is represented by horizontal fibers in the FDM mold; (B) The intermediate region containing randomly oriented cells and fibers is represented by a randomly oriented hexagonal pore structure; and (C) The deep region contains vertically aligned cells and fibers represented by orthogonal fibers in the FDM mold.

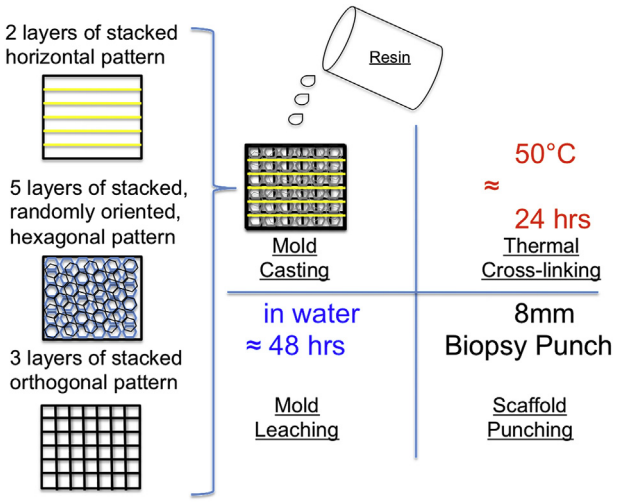

Fig. 2. Schematic illustration of the molds and osteochondral scaffold fabrication.

into the mold and cross-linked overnight in a 50 °C oven [12]. Based on our previous study [12], the PCL based resin with 96% R_f and 100% R_r has shown a favorable elastic modulus, transition temperature (21 °C) and recovery speed (23.1°/s) for our study. After cross-linking, heated sonication in water assisted in leaching the mold out of the bioink resin leaving a porous, channeled polymer structure. In addition, 5 g of nHA was incorporated into the bone layer of the PCL-based osteochondral constructs via a uniform deposition into the bottom of the empty scaffold molds before casting. Constructs were punched from this structure using an 8 mm biopsy punch. Moreover, one group of constructs underwent an additional fabrication step after punching to improve cartilaginous response. The upper half of these constructs, without nHA, was soaked in a dopamine hydrochloride solution to polymerize polydopamine (PDA) directly on the construct surface. The PDA coating facilitates highly efficient, simple immobilization of growth factors to the polymer surface [13]. After polymerization, the same half of these constructs was then soaked in bovine serum protein (BSA), to protect the activity of growth factor TGF-β1 to improve the spatial chondrogenic response.

2.3. Scaffold characterization

Optical microscopy was used to validate and examine complete leaching of the PVA material. Samples were left to air dry at room temperature for 2 h and viewed using a CM4210 Optical System with manual zoom (6.4 ×) and fine focus (656 × 492-pixel size) (DSA25, Kruss USA, Matthews, NC). Uniaxial unconfined compression testing was conducted on each sample group using an MTS Criterion Model 43 mechanical tester with a 1 kN load cell at a crosshead speed of 2 mm/min (n = 5, Applied Test Systems, Butler, PA). 8 mm samples were stored in ultrapure water and blotted dry prior to testing. The loads and displacements were continuously monitored during testing and employed to plot stress versus strain after complete. The Young's modulus was calculated from the slope of the elastic portion of the stress v. strain curve.

In addition, the temperature triggered shape memory effect was tested and realized through a series of steps outlined below. The constructs were first subjected to uniaxial compression using a small vice and held in the vice at 0 °C for 10 min. The vice was then released, and the compressed scaffold was held at 0 °C again for 10 min. The compressed scaffold was then removed from the freezer and the original shape was recovered using 37 °C water.

2.4. In vitro stem cell study

Primary human bone marrow mesenchymal stem cells (hMSCs) were obtained from healthy consenting donors and were thoroughly characterized at the Texas A&M Health Science Center, Institute for Regenerative Medicine. Complete media, composed of Alpha Minimum Essential medium (α-MEM, Gibco, Grand Island, NY), 16% fetal bovine serum (Atlanta Biologicals, Flowery Branch, GA), 1% L-Glutamine (Lonza, Walkersville, MD), and 1% penicillin:streptomycin (Gibco, Grand Island, NY), was used to culture hMSCs in a controlled environment at 5% CO_2/95% air and 37 °C. All studies used 3–6 cell passages. All constructs were sterilized for 30 min under UV light and then soaked for 15 min in 70% ethanol. Before seeding, samples were washed in phosphate-buffered solution (PBS) 2 times and pre-wet in PBS overnight.

Constructs were seeded at a density of 30,000 cells/scaffold for cell adhesion and proliferation studies. For adhesion, cell-seeded constructs were cultured for 4 h, removed from the culture environment, and transferred to a new well plate. For proliferation studies, samples were cultured for 1, 3, and 5 days in complete media. Samples were removed from the culture environment and transferred to new well plates for evaluation after respective time intervals. CellTiter 96 AQueous One Solution Cell Proliferation Assay (colorimetric MTS assay) was used to quantify adhesion and proliferation evaluations. Absorbance was measured at 490 nm wavelength.

For hMSC differentiation studies, constructs were seeded with 100,000 cells per scaffold and cultured in complete media supplemented with chondrogenic factors, including 100 ng/ml TGF-β1, for 1, 2, and 3 weeks, respectively. After each time point, constructs were transferred to a fresh well-plate and frozen at -80 °C for 24 h, lyophilized for 48 h, and digested in papain for 24 h at 60 °C.

Total collagen was quantified via Picro Sirius Red staining. Samples were analyzed by drying 100 μL of papain digestion in a well plate overnight. After drying, 150 μL of 0.1% Sirius Red in saturated Picric Acid was added to each well and incubated for 1 h at room temperature on an orbital shaker. Each well was then washed three times with 200 μL of 5% acetic acid. After the final wash, 150 μL of 0.1 M sodium hydroxide was added to each well, incubated at room temperature for 30 min, and analyzed with a photospectrometer at a wavelength of 550 nm.

Type II collagen was evaluated by double-antibody sandwich enzyme-linked immunosorbent assay (ELISA) (Fisher Scientific, Pittsburg, PA) per the manufacturer's instructions. Digested samples were added to 96-well plates pre-coated with purified human collagen type II antibody and incubated for 40 min. After incubation, each well was washed, and collagen type II specific detection antibody was added and incubated for 20 min, removed, and washed again. After washing, horseradish peroxidase (HRP)-Streptavidin enzyme conjugate was added to each well, incubated for 10 min, removed and washed. Samples were then incubated for 15 min after adding Tetramethylbenzidine (TMB) substrate to each well. Lastly, an acidic stop solution was added to the well plates and samples were read using an absorbance spectrophotometer at a wavelength of 450 nm.

Calcium deposition was measured using a calcium reagent kit (Pointe Scientific Inc., Canton, MI). Lysed constructs, as well as uncultured constructs were immersed in a 0.6 M hydrochloric acid solution at 37 °C for 24 h. Next, 20 μL of supernatant was mixed with 1 mL calcium colorant, o-cresolphthalein complexone. Once mixed, 100 μL of each sample was transferred to a 96 well-plate and read using an absorbance spectrophotometer at a wavelength of 570 nm.

All differentiation assays were normalized to cell density per scaffold. Cell density was quantified by a DNA PicoGreen assay and read by a fluorescent spectrophotometer with excitation and emission at 485 and 520 nm, respectively.

3. Statistical analysis

All data are represented as the mean value ± standard error of the mean and a student's t-test was used to evaluate differences among the groups. Student's t-test comparisons yielding $p < 0.05$ are considered statistically significant.

4. Results

4.1. Scaffold characterization and shape memory response

Fig. 3A shows the resultant constructs have well-defined architecture with distinguishable bone and cartilage parts. Constructs with nHA (nHA group in Fig. 3B and C) had a slightly improved mechanical performance over constructs without nHA (Bare group in Fig. 3B and C) when evaluated under compressive loading conditions, but the difference was not significant. The constructs coated with PDA (nHA + group in Fig. 3B and C), however, performed better than all other constructs for both the peak stress and Young's modulus. The increased compressive strength and modulus obtained with the constructs coated in PDA is beneficial for osteochondral, load-bearing applications in articulating joints such as the hip or knee.

The smart, PCL-based, constructs displayed favorable shape memory response with fixation at 0 °C and recovery at 37 °C. Still photographs of the recovery process are shown in Fig. 4 and the video is shown in the supplementary material.

Supplementary video related to this article can be found at https://doi.org/10.1016/j.bprint.2019.e00066

4.2. Enhanced hMSC adhesion and proliferation

To test the effectiveness of PDA coating and BSA/TGF-β1 modification, we first prepared the cartilage scaffold (top part on the final osteochondral scaffold) and examined the cell response to the modification. The cell adhesion and proliferation studies were firstly carried out. It was found that cell performance improved in samples with PDA and PDA + BSA/TGF-β1 compared to the bare PCL samples after 4 h of culture. Fig. 5 illustrates the favorable performance of the coated constructs supporting further evaluation through proliferation studies. The constructs with PDA outperformed the bare PCL controls significantly at all time points; the constructs with PDA + BSA/TGF-β1 outperformed all other constructs significantly at all time points, illustrated in Fig. 5B. PDA is a mussel-inspired polymerization process that improves cell attachment and growth. However, it can also inhibit extracellular matrix (ECM) formation over time; this challenge is overcome by introducing additional growth factors, in this case BSA and TGF-β1. Surface modifications and growth factor integration significantly improve the performance of the smart PCL-based bioink resins.

Confocal microscopy images further verified cellular growth, spreading morphology, and alignment on the PCL-based constructs (Fig. 6). Cellular attachment, spreading, and growth were evident after 5 days of culture on all scaffold materials, but modified scaffold material with nHA and/or BSA/TGF-β1 show greater quantity of cells and superior spreading. Fig. 6 also shows the favorable horizontal alignment of cells on the top layer of the printed constructs, similar to the orientation found on the surface of native articular cartilage.

4.3. Enhanced hMSC differentiation in cartilage constructs

Following the adhesion and proliferation studies, the chondrogenic differentiation of cartilage constructs was then investigated after 1, 2, and 3 weeks of culture. At the end of each culture time point, seeded constructs were evaluated for total collagen and type II collagen synthesis. Total collagen and type II collagen are also the two markers capable of showing the most distinction between chondrogenesis and osteogenesis when moving back into osteochondral evaluation in the future; this experiment strives to find an effective method for strengthening these markers.

Total collagen synthesis, illustrated in Fig. 7A, was assessed for hMSC differentiation. As a late-stage marker of extracellular matrix formation, total collagen serves as an indicator of scaffold biocompatibility. The constructs with PDA and BSA/TGF-β1 outperformed all other constructs significantly in week 3 by approximately 18%. Type II collagen was also evaluated for chondrogenic differentiation. Fig. 7B shows the synthesis of the type II collagen. Samples with PDA + BSA/TGF-β1 significantly outperformed all other constructs yielding approximately 50% more total collagen after 3 weeks of culture.

4.4. Enhanced hMSC differentiation in osteochondral constructs

After evaluation of PDA coating effectiveness with cartilage constructs, we performed the hMSC osteochondral differentiation test with the entire osteochondral constructs. Total collagen synthesis, that includes osteogenesis marker type I collagen and chondrogenesis marker type II collagen, was assessed for hMSC osteochondral differentiation. For the complete scaffold evaluation, the scaffold with nHA, PDA, and TGF-β1 outperformed all other constructs in week 3 by 12.5%, Fig. 8A. In addition, to evaluate the scaffold as a whole, constructs were also sliced at midsection into top cartilage portion and bottom bone portion to evaluate the differentiation separately. In the sliced data, the bottom half of each scaffold outperformed the upper half in all groups by week 3.

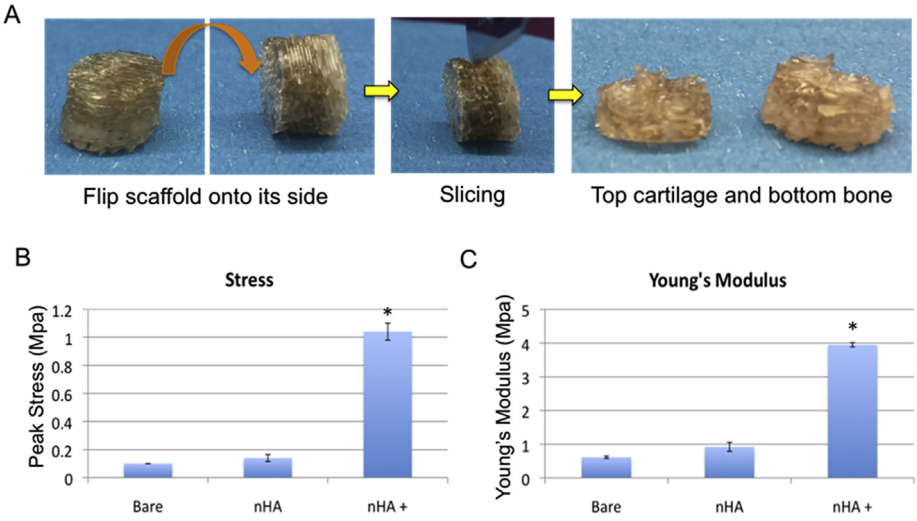

Fig. 3. (A) Photographic images depicting the resultant scaffold and the sliced biphasic structure. (B) Average compression test results for peak stress, and (C) Young's moduli of various constructs. Significantly higher peak stress and Young's modulus is noted on the osteochondral constructs with nHA, PDA and BSA/TGF-β1 (nHA + group). Data are the mean ± standard error of the mean, n = 5, *p < 0.05.

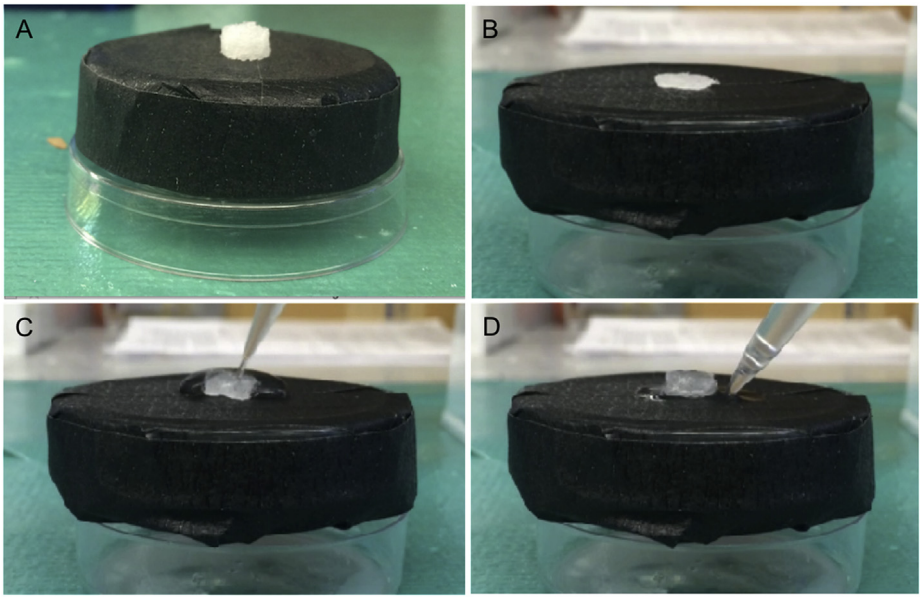

Fig. 4. Time-lapse images of the shape memory response of the scaffolds. (A) Undeformed scaffold; (B) Deformed Scaffold; (C) scaffold mid-recovery; (D) Fully recovered scaffold.

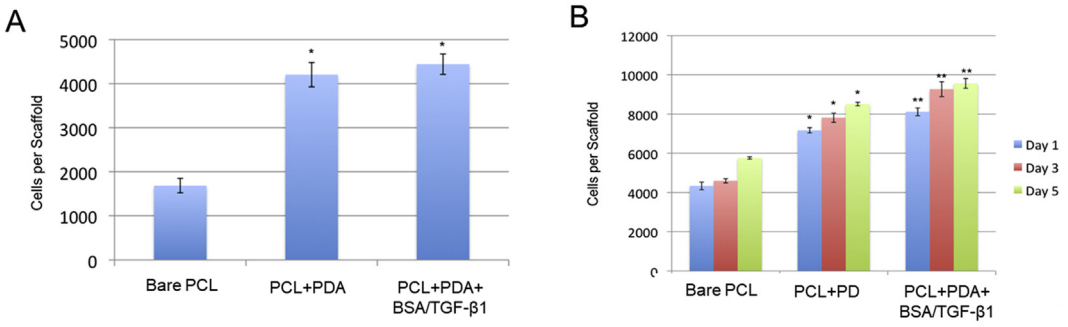

Fig. 5. (A) Enhanced hMSC adhesion and (b) proliferation in various 3D printed, PCL-based constructs. Constructs coated in PDA outperformed the bare control scaffold significantly (*$p < 0.05$) at all time points. Constructs coated with PDA and BSA/TGF-β1 significantly outperform all other constructs at all time points (**$p < 0.05$). Data are the mean ± standard error of the mean, $n = 9$.

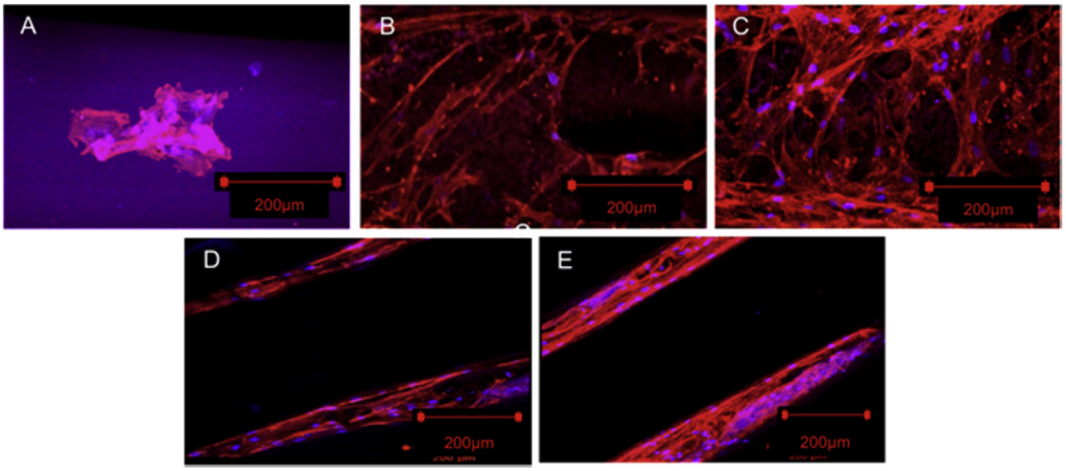

Fig. 6. Confocal microscope images of PCL-based polymer and printed scaffolds after 5 days of culture. (A) Bare PCL-based materials; (B) PCL-based materials coated with PDA; (C) PCL-based materials coated with PDA and BSA/TGF-β1. The PDA and bioactive factor modification can improve cell attachment and growth. (D) Printed PCL-based scaffolds with PDA; (E) printed PCL-based scaffolds with PDA and BSA/TGF-β1. Both 3D printed scaffolds depicted above show good cell attachment, growth, as well as alignment within designed scaffold channels.

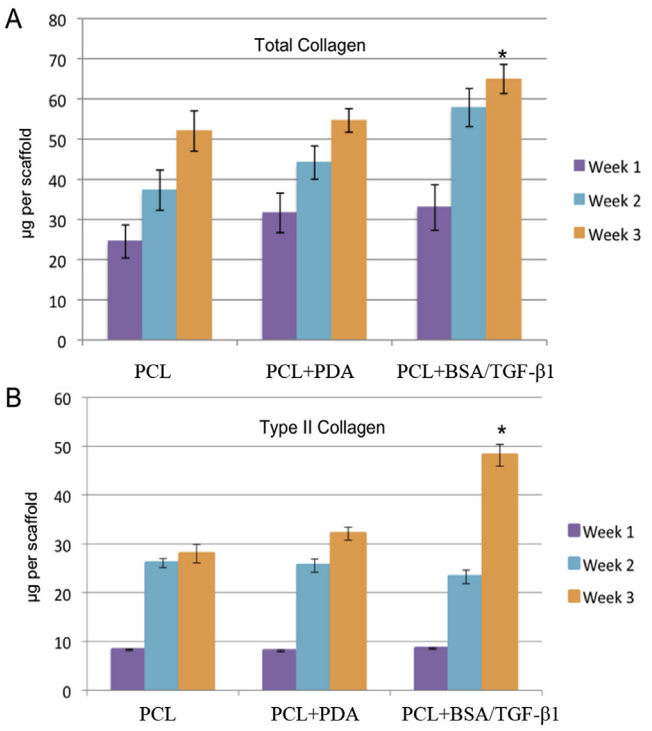

Fig. 7. (A) Total collagen synthesis. After 2 and 3 weeks of culture the constructs coated with PDA and BSA/TGF-β1 had a higher total collagen content (*$p < 0.05$) when compared to other constructs. (B) Type II collagen synthesis. After 3 weeks of culture, the constructs coated with PDA and BSA/TGF-β1 had significantly higher levels of Type II Collagen (*$p < 0.05$) when compared to all other constructs with. Data are the mean ± standard error of the mean, n = 9.

Additionally, the constructs with nHA and those with nHA, PDA, and TGF-β1 significantly outperformed all other constructs in total collagen production on the top half, in week 3, by at least 14%, Fig. 8B.

Extracellular calcium is an important marker for late-stage osteogenic differentiation. The contribution of calcium due to incorporated nHA was accounted for and all data were normalized to remove these effects. Constructs containing nHA outperformed constructs without nHA with at least 75% higher concentration of calcium at all time points. The bottom half of constructs supplemented with PDA and TGF-β1 performed significantly better than all other constructs, by at least 13%, in week 3, Fig. 9.

5. Discussion

Scaffold geometry and architecture are important for guiding cellular alignment and distribution in a way that mimics the natural arrangement of cells in the human body [14–17]. In this study, we created a gradient structure, where the pore distribution varies vertically to mimic the natural gradients present in osteochondral tissue. At the surface of all articulating joints, two pairs of tissue (the ball and socket) meet and must interact smoothly to prevent continued wear and injury. Guiding cellular alignment and ECM formation at these surfaces is critical and was achieved in this study as demonstrated by the results in Fig. 6. This cellular alignment was realized through the versatility of 3D bioprinting using FDM and the investment casting process. This successful process can be further refined to better mimic the architecture of this region by incorporating appropriate spatial distributions as well as alignment. This printing technique, and its supporting software, provide great flexibility to readily tune and scale scaffold microfeatures that subsequently affect scaffold biological and mechanical performance. Porous designs not only increase usable space on the constructs by increasing surface area, they also act as guides for cellular attachment and spreading. PCL-based bioink resins, employed through the investment casting process, further illustrate the versatility of this procedure. Numerous options exist for curable bioinks integrated through investment casting.

Though not fully investigated in this experiment, the shape changing behavior of this scaffold brings promise for minimally invasive cartilaginous implantation for near-surface, non-load bearing, applications [18, 19]. Also, the elastic nature of this material is favorable for a dynamically responsive implant promoting cellular response through internal shear stresses and mechanical responses. Both of these potential benefits of this type of scaffold warrant further investigation.

For hMSC differentiation, PDA and BSA/TGF-β1 were integrated into the constructs to evaluate their contribution toward chondrogenic differentiation of hMSCs for improved cartilage regeneration. After the scaffold mold is leached and constructs are punched, biological markers or growth factors can be added to the surface with various polymerization and soaking techniques. The amount of bioactive material incorporated in bioinks or applied to surfaces is tunable, further improving the flexibility of the resultant scaffold design.

Chondrogenic biological assays were conducted to evaluate cellular response in each scaffold. Fig. 7 indicates that the addition of PDA + TGF-β1 significantly improves the chondrogenic response of the constructs. The flexibility of the FDM 3D bioprinter, and the investment casting process, support the extensive manipulation of geometries as well as incorporation and distribution of nano-micro-particles post fabrication. The current work uniformly incorporates chondrogenic markers to evaluate their potential for increasing chondrogenesis over a bare scaffold soaked in chondrogenic media. The placement of markers was uniform over the full thickness of the scaffold but could be spatially distributed for applications within the osteochondral region.

Through compression testing with the PCL-based constructs, a small increase was noted in nHA-containing constructs, however, a much more significant improvement was noted in those coated with PDA. The mechanism behind the positive impact of PDA coatings and thin films on the mechanical performance of substrate materials is currently not well-understood [20]. Based on our testing, the constructs containing nHA fractured in shear at the mid-point, similar to a delamination

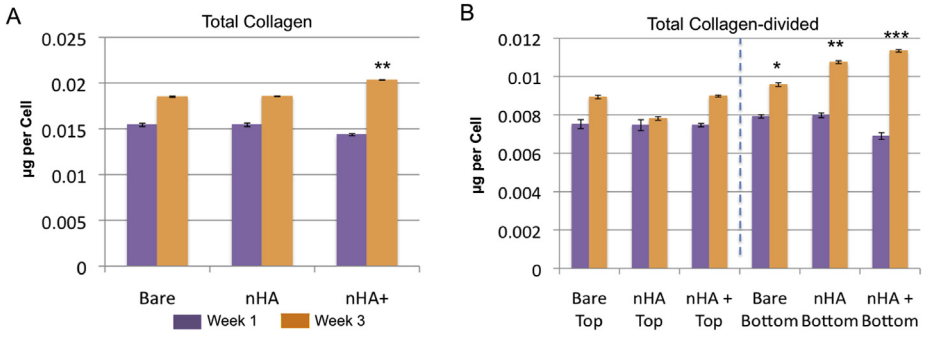

Fig. 8. (A) Total collagen synthesis, after 3 weeks of culture, constructs coated with PDA and BSA/TGF-β1 performed significantly better than other groups (**$p < 0.05$). (B) The bottom half of the constructs outperformed the top significantly by week 3 in all groups (*$p < 0.05$), constructs coated with PDA showed significantly greater total collagen synthesis on the bottom halves compared to all other groups (**$p < 0.05$), and the constructs with PDA and BSA/TGF-β1 outperformed all constructs significantly on the bottom half (***$p < 0/.05$). Data are the mean ± standard error of the mean, n = 6.

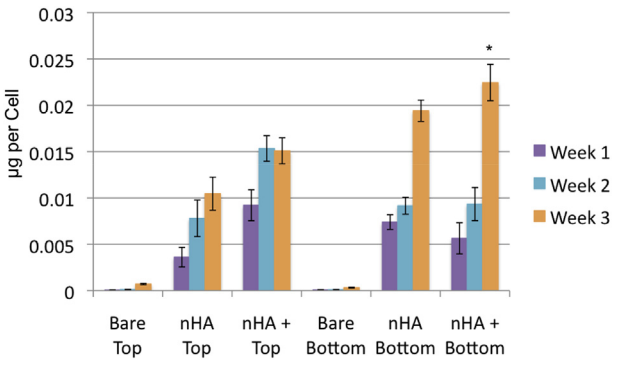

Fig. 9. Total calcium synthesis. After 3 weeks of culture the constructs coated with PDA and BSA/TGF-β1 had a higher calcium content (*$p < 0.05$) when compared to constructs with only nHA and bare constructs without augmentation. Data are the mean ± standard error of the mean, n = 6.

effect. But the constructs coated with PDA did not show any evidence of shear or delamination and had not fractured when testing ending at 50% strain. This may contribute to the improved mechanical performance.

In addition to the good mechanical performance noted with the PDA-coated constructs with nHA, the cellular performance was also significantly better when considering the balance of the osteogenic and chondrogenic response over the full thickness of the scaffold. For hMSC differentiation, nHA alone was integrated into one group of PCL-based constructs while another group had nHA and was further coated with PDA and TGF-β1, while the control scaffold was bare PCL. After the scaffold mold was 3D printed, the liquid resin was manipulated prior to investment casting with nHA in half of the mold for a spatial osteogenic influence. After cross-linking, one group underwent surface modifications coating with PDA first, followed by TGF-β1.

Also, a challenge with this experiment is the limitation on size of the constructs. To replicate the osteochondral region, constructs must be at least 3–4 mm in size [21]. Static culture of such a robust scaffold is challenging. Integrating a bioreactor would significantly improve long term cell survival and move this concept forward for future *in vivo* analysis [22].

6. Conclusion

A major goal of this research was to find a novel biomaterial that supports a chondrogenic and osteogenic response for osteochondral tissue fabrication. Improved biological performance was achieved on porous PCL-based smart polymer constructs with PDA + TGF-β1 when compared to the bare constructs and constructs coated with PDA only. The region with nHA does increase hardness and stiffness, favorable for the bone side of the scaffold, without compromising the soft, pliable side of the scaffold targeting a cartilaginous response. The successful biological response of coated constructs, coupled with the favorable shape memory response of the novel material, show great promise for further investigations targeting both cartilaginous and osteochondral responses.

Acknowledgments

The authors would like to thank the financial support from NSF BME program grant # 1510561.

References

[1] N.J. Castro, J. O'Brien, L.G. Zhang, Integrating biologically inspired nanomaterials and table-top stereolithography for 3D printed biomimetic osteochondral scaffolds, Nanoscale 7 (2015) 14010–14022.
[2] B.A. Harley, A.K. Lynn, Z. Wissner-Gross, W. Bonfield, I.V. Yannas, L.J. Gibson, Design of a multiphase osteochondral scaffold III: fabrication of layered scaffolds with continuous interfaces, J. Biomed. Mater. Res. A 92A (2010) 1078–1093.
[3] N.J. Castro, S.A. Hacking, L.G. Zhang, Recent progress in interfacial tissue engineering approaches for osteochondral defects, Ann. Biomed. Eng. 40 (2012) 1628–1640.
[4] K. Ye, C. Di Bella, D.E. Myers, P.F.M. Choong, The osteochondral dilemma: review of current management and future trends, ANZ J. Surg. 84 (2014) 211–217.
[5] M.A. Nowicki, N.J. Castro, M.W. Plesniak, L.G. Zhang, 3D printing of novel osteochondral scaffolds with graded microstructure, Nanotechnology 27 (2016), 414001.
[6] X. Zhou, T. Esworthy, S.-J. Lee, S. Miao, H. Cui, M. Plesiniak, et al., 3D Printed scaffolds with hierarchical biomimetic structure for osteochondral regeneration, Nanomed. Nanotechnol. Biol. Med. (2019), https://doi.org/10.1016/j.nano.2019.04.002.
[7] B. Holmes, W. Zhu, J. Li, J.D. Lee, L.G. Zhang, Development of novel three-dimensional printed scaffolds for osteochondral regeneration, Tissue Eng. A 21 (2014) 403–415.
[8] H. Cui, M. Nowicki, J.P. Fisher, L.G. Zhang, 3D bioprinting for organ regeneration, Adv. Healthc. Mater. 6 (2017), 1601118.
[9] J. Korpela, A. Kokkari, H. Korhonen, M. Malin, T. Närhi, J. Seppälä, Biodegradable and bioactive porous scaffold structures prepared using fused deposition modeling, J. Biomed. Mater. Res. B Appl. Biomater. 101B (2013) 610–619.
[10] W. Zhu, M. Wang, Y. Fu, N.J. Castro, S.W. Fu, L.G. Zhang, Engineering a biomimetic three-dimensional nanostructured bone model for breast cancer bone metastasis study, Acta Biomater. 14 (2015) 164–174.
[11] W. Zhu, N.J. Castro, H. Cui, X. Zhou, B. Boualam, R. McGrane, et al., A 3D printed nano bone matrix for characterization of breast cancer cell and osteoblast interactions, Nanotechnology 27 (2016), 315103.
[12] S. Miao, W. Zhu, N.J. Castro, J. Leng, L.G. Zhang, Four-Dimensional printing hierarchy scaffolds with highly biocompatible smart polymers for tissue engineering applications, Tissue Eng. C Methods 22 (2016) 952–963.
[13] K. Yang, J.S. Lee, J. Kim, Y.B. Lee, H. Shin, S.H. Um, et al., Polydopamine-mediated surface modification of scaffold materials for human neural stem cell engineering, Biomaterials 33 (2012) 6952–6964.
[14] W. Zhu, B. Holmes, R.I. Glazer, L.G. Zhang, 3D printed nanocomposite matrix for the study of breast cancer bone metastasis, Nanomed. Nanotechnol. Biol. Med. 12 (2016) 69–79.
[15] S.M. Giannitelli, D. Accoto, M. Trombetta, A. Rainer, Current trends in the design of scaffolds for computer-aided tissue engineering, Acta Biomater. 10 (2014) 580–594.
[16] A. Graziano, R. d'Aquino, M.G.C.-D. Angelis, F. De Francesco, A. Giordano, G. Laino, et al., Scaffold's surface geometry significantly affects human stem cell bone tissue engineering, J. Cell. Physiol. 214 (2008) 166–172.
[17] A.A. Zadpoor, Bone tissue regeneration: the role of scaffold geometry, Biomater. Sci. 3 (2015) 231–245.
[18] H. Cui, S. Miao, T. Esworthy, S. Lee, X. Zhou, S.Y. Hann, et al., A novel near-infrared light responsive 4D printed nanoarchitecture with dynamically and remotely controllable transformation, Nano. Res. 12 (2019).
[19] S. Miao, N. Castro, M. Nowicki, L. Xia, H. Cui, X. Zhou, et al., 4D printing of polymeric materials for tissue and organ regeneration, Mater. Today 20 (2017) 577–591.
[20] V. Ball, D. Del Frari, M. Michel, M.J. Buehler, V. Toniazzo, M.K. Singh, et al., Deposition mechanism and properties of thin polydopamine films for high added value applications in surface science at the nanoscale, BioNanoScience 2 (2012) 16–34.
[21] S.-J. Seo, C. Mahapatra, R.K. Singh, J.C. Knowles, H.-W. Kim, Strategies for osteochondral repair: focus on scaffolds, J. Tissue Eng. 5 (2014), 2041731414541850.
[22] H. Cui, W. Zhu, B. Holmes, L.G. Zhang, Biologically inspired smart release System based on 3D bioprinted perfused scaffold for vascularized tissue regeneration, Adv. Sci. 3 (2016), 1600058.